

## Experimental research on free-surface vortices as transport mechanism in wastewater sumps

Clemens, Francois; Duinmeijer, Alex

**Publication date**

2016

**Document Version**

Accepted author manuscript

**Published in**

8 th International Conference on Sewer Processes and Networks

**Citation (APA)**

Clemens, F., & Duinmeijer, A. (2016). Experimental research on free-surface vortices as transport mechanism in wastewater sumps. In *8 th International Conference on Sewer Processes and Networks: August 31 –September 2, 2016, Rotterdam, The Netherlands*

**Important note**

To cite this publication, please use the final published version (if applicable). Please check the document version above.

**Copyright**

Other than for strictly personal use, it is not permitted to download, forward or distribute the text or part of it, without the consent of the author(s) and/or copyright holder(s), unless the work is under an open content license such as Creative Commons.

**Takedown policy**

Please contact us and provide details if you believe this document breaches copyrights. We will remove access to the work immediately and investigate your claim.

---

## Experimental research on free-surface vortices as transport mechanism in wastewater sumps

Alex Duinmeijer<sup>1,2</sup>, Francois Clemens<sup>1,3</sup>

<sup>1</sup>Water Management Department, Faculty of Civil Engineering and Geosciences, University of Technology Delft (Email: [spa.duinmeijer@rotterdam.nl](mailto:spa.duinmeijer@rotterdam.nl))

<sup>2</sup>Municipality of Rotterdam, The Netherlands

<sup>3</sup>Deltares, The Netherlands

### Abstract

Sumps of wastewater pumping station can experience problems due the formation of (solid) floating layers of fat and scum as a result of insufficient current guidelines for sump design with respect to transport of floating debris. To complimentary the guidelines, the use of free-surface vortices is defined as a potential transport mechanism for floating debris. The transport ability and capacity of vortices is investigated in an experimental set-up and experimental data will be used to design and validate a theoretical vortex transport model describing the transport ability and capacity of a free-surface vortex. Two theoretical vortex models describing the vortex flow field are used as a base for the transport model. Experimental results show that both models needs adaptation to match experimental results. Furthermore, the experiments show that the ability to transport buoyant material is highly sensitive on the flow field in the vortex (core) and on the particle density. Particles can either get stuck in the vortex core with no or less transport or either translated around the core with efficient transport. Before designing and validating the vortex transport model, extensive future research is needed to capture the observed phenomena's.

### Keywords

Wastewater, pumping station, scum layers, free-surface vortex transport, experiments

## INTRODUCTION

Wastewater pumping stations can experience problems due to the presence of floating fat and scum in the pump sump. The presence of this floating debris can result in pump failures, which may result in a 16% increase of yearly volume of CSO's as shown by Korving (2006b) for a specific case study. The current guidelines for sump design (e.g. ANSI/HI, 2012) only deal with the transport of floating debris in a superficial manner and for a limited number of sump geometries.

To complement the guidelines with respect to the transport of floating debris, the authors have started a research on the mechanisms of formation and degradation of debris layers. They defined two mechanisms for transport of floating debris (1) by keeping floating particles in suspension and (2) the use of free-surface vortices for transport of floating debris from the water surface to the suction inlet. To investigate the mechanism of transport by free-surface vortices, the author developed an experimental-setup in which (strong) free-surface vortices are generated to investigate their ability and capacity of transporting floating material. The experimental data will be used for designing and validating a theoretical vortex transport model. The aim of this model is (1) to predict the transport capacity and efficiency of free-surface vortices as function of the present hydraulic conditions in existing wastewater pump sumps and (2) to provide design conditions in the design stage of new sumps. Before designing and validation of the transport model, extensive measurements are

conducted to analyse in a qualitative way the vortex characteristics and the ability to transport buoyant particles. This paper focusses on the description of the experimental set-up, methods and a qualitative description of the observed vortex flow and transport characteristics. The paper starts with mathematical description of the free-surface vortex and two different vortex models are presented which velocity formulae forms the base of the free surface vortex transport model.



**Figure 1** The presence of a closed floating layer of scum and fat in a wastewater pump sump (Rotterdam, 2014)

### THE FREE-SURFACE VORTEX

The background of using free-surface vortices as an mechanism to transport debris from the water surface to the pump inlet, is based on the presence of vertical velocities in the vortex giving a downwards vertical drag on the particles. This type of vortex which, for example, can be observed by emptying a bath-tub or sink and is characterized by high tangential velocities near its centre resulting in a water surface depression defined as the aircore depth  $H_D$ . Physically, this vortex is characterized by an outer field of irrotational flow with no vorticity in it and an inner vortex core of solid-body rotation in where all the vorticity is concentrated, see Figure 2.

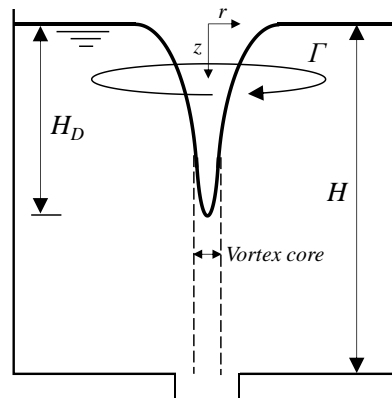


**Figure 2** General free-surface vortex model consisting of irrotational outer field and solid-body rotating inner vortex core

A classical mathematical model to describe the tangential or circumferential flow velocity in both the outer field and inner core was proposed by Rankine (1858) and consist of two separate equations:

$$\begin{aligned}
 V_{\theta} &= \omega r \quad (r < r_c) \\
 V_{\theta} &= \frac{\Gamma}{2\pi r} \quad (r > r_c)
 \end{aligned}
 \tag{1}$$

where  $V_{\theta}$  the tangential velocity,  $r$  the radius,  $\omega$  the angular velocity of the solid-body,  $\Gamma$  the (bulk) circulation of the outer flow field and  $r_c$  the radius representing the position of the transition between the inner core and the outer field. At  $r = r_c$  Eq. (1) has a discontinuity giving infinite high velocities.

### Burgers/Odgaard vortex model

Based on the Navier-Stokes equations governing viscous flow and the assumption that the radial velocity  $V_r = -ar$ , Burgers (1948) derived an expression for the velocities considering viscous dissipation of vorticity which is not included in the Rankine model. The Burgers model has no discontinuity at  $r = r_c$  and is an outstanding example of the balance between convection, intensification and diffusion of vorticity:

$$\begin{aligned}
 V_{\theta} &= \frac{\Gamma}{2\pi r} \left[ 1 - \exp\left(-1.25 \frac{r^2}{r_c^2}\right) \right] = \frac{\Gamma}{2\pi r} \left[ 1 - \exp\left(-\frac{ar^2}{2\nu_t}\right) \right] \\
 V_r &= -ar \\
 V_z &= 2az
 \end{aligned}
 \tag{2}$$

with  $a \sim \partial V_z / \partial z$  the (constant) suction parameter and  $\nu_t$  the total viscosity containing both kinematic and eddy viscosity and will be discussed later. The effect of viscous diffusion is counteracted by axial stretching of the vortex core intensifying the core vorticity. At bath-tubs or intake structures, this stretching is driven by the accelerating flow towards the suction inlet. However, the assumption of  $V_r = -ar$  counts only for the inner core assuming no radial gradient of axial velocity ( $\partial V_z / \partial r = 0$ ) which is questionable as discussed later. The Burgers exponential expression of the tangential velocity matches very good with experimental results but the exponential expression in equation has no analytical solution and makes it difficult to use the equation for further analysis.

### Hite and Mih vortex model

Mih (1991) modified the Rosenhead (1930) formula to get the follow expression for the tangential and axial velocity distribution (from Hite and Mih, 1994):

$$\begin{aligned}
 V_{\theta} &= \frac{\Gamma_{\infty}}{2\pi r_c} \frac{2R}{1 + 2R^2} \\
 V_r &= -\frac{\nu_t}{r_c} \frac{8R}{(1 + 2R^2)} \\
 V_z &= \frac{\nu_t}{r_c^2} \frac{16z}{(1 + 2R^2)^2}
 \end{aligned}
 \tag{3}$$

with  $R$  the nondimensional radial coordinate  $r/r_c$ . This formula approximates Eq. (2) but the maximum velocity of Eq. (3) occurs at  $R = 0.71$  instead of  $R = 1$  as showed by numerous experimental data. However, Eq. (3) is much easier to use in further analysis.

### Calculation of aircore depth

Now, by using the expression of the radial momentum from the axisymmetric laminar Navier-Stokes equation

$$V_r \frac{\partial V_r}{\partial r} + V_z \frac{\partial V_r}{\partial z} - \frac{V_\theta^2}{r} = -\frac{1}{\rho} \frac{\partial p}{\partial r} + \nu \left( \frac{\partial^2 V_r}{\partial r^2} + \frac{1}{r} \frac{\partial V_r}{\partial r} - \frac{V_r}{r^2} + \frac{\partial^2 V_r}{\partial z^2} \right) \quad (4)$$

and assuming that the radial and axial velocity is small compared to the tangential velocity (i.e. Anwar (1966)) so  $V_\theta^2 \gg V_r^2$  and that the pressure in z-direction is hydrostatic (e.g. Odgaard (1986), Gulliver (1987) and Suerich-Gulick (2014a)), the pressure distribution can be expressed as:

$$p(r, z) = \rho g z + \int_0^r \rho \frac{V_\theta^2}{r} dr \quad (5)$$

The surface tension pressure  $p_s$  at the tip of the aircore is of a magnitude of  $-2\sigma/r_c$  and its contribution to the aircore depth in this research is of an order of  $10^{-3}$  m and assumed as negligible (Odgaard 1986). Now, by choosing the z-coordinate at the tip of the aircore where the pressure  $p(0, z)$  and integrating from  $r = 0$  to  $r = \infty$ , the total aircore depth  $H_D = p/\rho g$  is than given by:

$$H_D = \frac{1}{g} \int_0^\infty \frac{V_\theta^2}{r} dr \quad (6)$$

### Burgers/Odgaard model

By substituting the Burgers tangential velocity in Eq. (2) in Eq. (6) the total aircore depth is calculated by:

$$H_D = \frac{1}{g} \left( \frac{\Gamma}{2\pi} \right)^2 \int_0^\infty \left( 1 - \exp\left( \frac{-ar^2}{2\nu_t} \right) \right)^2 r^{-3} dr \quad (7)$$

As proposed by Odgaard (1986) the suction parameter  $a$  is determined by using the Burgers axial velocity equation  $V_z = 2az$  and taking  $V_z$  as the average velocity in the outlet thus  $z = H$  and:

$$a = \frac{2Q}{\pi D^2 H} \quad (8)$$

By substituting Eq. (8) in Eq. (7),  $H_D$  can be solved by for example numerical integration.

### Hite & Mih model

By substituting the tangential velocity Eq. (3) in Eq. (6) and taking  $R \rightarrow \infty$ , the total aircore depth  $H_D$  is calculated by:

$$H_D = \frac{1}{g} \left( \frac{\Gamma}{2\pi r_c} \right)^2 \quad (9)$$

The core radius  $r_c$  can be derived from the axial velocity equation in Eq. (3):

$$r_c = \sqrt{\frac{16\nu_t z}{V_z(1 + 2R^2)^2}} \quad (10)$$

The core radius can be calculated by assuming the average velocity  $U_i$  in the outlet as the maximum axial velocity  $V_z$  at the core centre ( $R = 0$ ) which is analogue as proposed by Odgaard (1986) using the Burgers model. By substituting Eq. (10) in Eq. (9),  $H_D$  is calculated by:

$$H_D = \frac{0.0625\Gamma^2 Q}{g\pi^3\nu_t D^2 H} \quad (11)$$

### Eddy viscosity

At high values of  $\Gamma$  and thus large tangential velocities near the vortex core, there will be a transition of laminar to turbulence flow at the core. The high shear stresses due to the tangential velocity gradients  $\partial V_\theta/\partial r$  near the core generate turbulence and thus an increasing of viscous dissipation. Beside kinematic viscosity  $\nu$ , the flow will then also be controlled by eddy viscosity  $\varepsilon$  and thus  $\nu_t = \nu + \varepsilon$ . Based on Prandtl's mixing-length theory, Odgaard (1986) suggested that the eddy viscosity  $\varepsilon$  is proportional to  $\partial V_\theta/\partial r$  with  $\partial V_\theta/\partial r \gg \partial V_z/\partial r$  and  $\partial V_\theta/\partial r \gg \partial V_r/\partial r$ . Now, according to Odgaard (1986), as it is reasonable to expect proportionality between  $\varepsilon$  and  $V_{\theta c} r_c$  or between  $\varepsilon$  and  $\Gamma$ ,  $\varepsilon$  can be calculated by  $\varepsilon = k\Gamma$  with  $k$  a proportionality factor estimated as  $k \approx 6 \times 10^{-5}$  (Odgaard 1986). Regarding this research, both the Burgers/Odgaard as the Hite & Mih model uses the expression  $\nu_t = \nu + k\Gamma$ .

## EXPERIMENTAL SET-UP

### General description

The experimental set-up consists of a transparent tank of 0.60 m diameter and 1.0 m high. The tank is placed in a 0.7 x 0.7 m transparent container to compensate light refraction when recording images. The set-up is a closed system with a pump discharging water in the tank that flows through an outlet in the bottom back to the pump. To investigate the influence of the outflow axial velocity on the vortex characteristics, the set-up is used with three outlet pipe diameters: 0.030 m, 0.044 m and 0.060 m. A separation tank of 0.3 x 0.3 x 0.4 m is placed between the tank outlet and the pump suction side for separating experimental floating particles from the closed system. The flow rate is measured with a Kobold Magnetic-Inductive Flowmeter model DMH. The flow enters the tank through two horizontal Ø25.9 x 1.9 mm inlet pipes located adjacent to the tank wall and 0.5 m above the tank bottom. To vary the flow circulation  $\Gamma$  which is a governing parameter in strong vortex formation, the pipes are rotatable about their long axis affecting the angle of inflow in the horizontal plane. The circulation is more varied by vary the distribution of the total flowrate over both pipes by adjusting the flowrate of one pipe with a control valve.

### Evaluating geometrical effects on vortex flow

The presence of the pipes may not result in a radial gradient of the circulation and therefore the influence is investigated with a two-phase CFD-model of the experimental set-up. The model mesh

consists of two-million cells and the geometry includes both inflow pipes and a laminar approach is used. The calculated circulation is about the same as the measured circulation with nearly no radial gradient of the circulation  $\partial\Gamma/\partial r$  outside the vortex. Based on this flowrate we may conclude that the presence of the pipes does not lead to a radial gradient of the circulation and that the method of measuring the (bulk) circulation  $\Gamma_\infty$  is assumed as valid. From the CFD results, it was also shown that the inflow jet reached until the tank bottom however with very low velocities. As the presence of a radial boundary layer flow could play an important role in the vortex characteristics (e.g. Echávez 2002), the jet flow may not affect this boundary layer. This effect is evaluated by replacing the individual  $\text{Ø}25$  mm nozzle by nine  $\text{Ø}10$  mm nozzles reducing the inflow velocities with a magnitude of about 40% and comparing the measured aircore depth between both inflow configurations at same hydraulic conditions i.e. outlet diameter, undisturbed water depth, flow rate and circulation. This is completed for 16 different combinations of flow rate. The differences in measured aircore depths are negligible hence, the assumption is made that the jet formation is not affecting the radial bottom boundary layer.

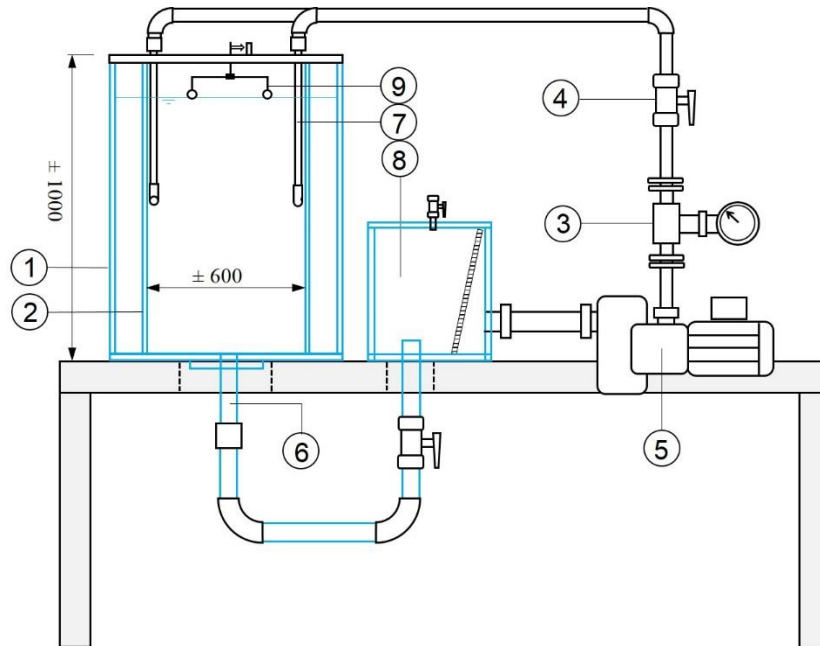


**Figure 3** Experimental set-up with (1) transparent container of 0.7 x 0.7 x 1.0 m (2)  $\text{Ø}600$  mm x 1000 mm transparent tank, (3) magnetic flow meter, (4) control valve, (5) pump (6) outlet pipe (0.03, 0.044 and 0.06 m), (7)  $\text{Ø}25$  mm inlet pipes, (8) Separation tank and (9) floating quadripod with magnetic pulse recording.



**Figure 4** Left photo: Ø600 mm x 1000 mm vortex tank with strong free-surface vortex. Right photo: separation tank to separate transported material from the flow circulating in the system.

### Determining of bulk circulation

As also used by Brocard (1983) and Echávez (2002), the bulk circulation is determined by measuring the circumferential velocity with a floating quadripod consisting of four egg shaped hollow balls connected to a 0.30 m cross shaped frame of 3 mm diameter aluminium rods.



**Figure 5** Left: floating quadripod to determine flow circulation consisting of four egg shaped hollow balls connected to a 0.30 m cross shaped frame of 3 mm diameter aluminium rods. Right: magnetic device recording the quadripod revolution rate.

This method is based on the Stokes' theorem saying that the bulk circulation  $\Gamma_\infty$  is the integral of the axial vorticity  $\omega_z$  across the cross-sectional area of the tank and equal to the line integral of the tangential velocity  $V_\theta$  around a closed circle  $C$  with radius  $r$  enclosing the vortex area:

$$\Gamma = \oint_C \vec{V} d\vec{l} = 2\pi r V_{\theta,r} \quad (12)$$

As the bulk vorticity is concentrated in the vortex core ( $r < r_c$ ) the calculation of the line integral must be conducted at relatively large radius from the vortex core. The measuring of  $V_\theta$  is conducted at a distance  $r = 0.15$  m which is much larger than  $r_c$ , and thus assumed as valid to determine  $\Gamma_\infty$ . The  $V_\theta$  is calculated by measuring the quadripod revolution rate  $N$  and the corresponding circulation is then calculated by  $\Gamma = N(\pi d)^2/t$  where  $d = 0.3$  m the diameter of the quadripod and  $t$  the measured time to accomplish  $N$  revolutions.

### Visualisation of vortex characteristics

The visualisation of the vortex flow and movement of experimental floating particles is recorded by an iPhone 8-megapixel iSight-camera (1080p). This camera is particularly used because of the 120 fps slow motion function required to use PIV-techniques and analysing the vertical transport of floating particles.

### Uncertainty analysis

The measured parameters are used to calculate theoretical model results and comparing them with experimental results. Hence, the model confidence interval  $\delta H_D$  must be known. Based on preliminary research, the Hite & Mih (1994) model gives a better math with experimental results and therefore the confidence interval is only derived for this model.

#### Parameter uncertainty

The measuring accuracy of the flow meter is  $\pm 0.3$  % of actual value +  $0.0001 * Q$  at 10 m/s. Based on the DN25 diameter, the total accuracy is then  $\pm(0.003Q + 0.0018)$  m<sup>3</sup>/h. During experiments the measured flow rate fluctuates with a deviation of about 0.02 m<sup>3</sup>/h. This deviation is included in the uncertainty calculation giving a maximal total uncertainty of  $\delta Q = \pm(0.003Q + 0.02)$  m<sup>3</sup>/h. The (undisturbed) water depth  $H$  is measured with a rule and the uncertainty in reading the rule is defined as 0.002 m. However, due to the presence of the volume of the aircore, the water depth will increase because of conservation of mass. From initial experiments, the maximum variation is about 0.01 m. This value is much higher than the rule uncertainty and therefore defined as the uncertainty  $\delta H$ . The diameter  $D$  is a constant parameter with a defined uncertainty  $\delta D = 0.001$  m. Uncertainties in the circulation calculation  $\Gamma = N(\pi d)^2/t$  are introduced by inaccuracies in the quadripod length  $d$  and the time registration  $t$  by stopping the stopwatch. The first is defined as  $\delta d = 0.002$  m and the latter by some tests as  $\delta t = 0.3N$ . Based on these numbers, the uncertainty  $\delta \Gamma$  in calculation the circulation is:

$$\delta \Gamma = \sqrt{\left(\left|\frac{\partial \Gamma}{\partial d}\right| \delta d\right)^2 + \left(\left|\frac{\partial \Gamma}{\partial t}\right| \delta t\right)^2} = \Gamma \sqrt{0.0002 + \frac{0.09N^2}{t^2}} \approx 0.1\Gamma$$

Each circulation is calculated by  $N = 5$  and the lowest measured total time  $t$  is about 15 s. Therefore, the uncertainty in calculation the circulation is simplified to a maximum of  $0.1\Gamma$ . As the contribution of the eddy viscosity is an order of magnitude 5 times larger than the kinematic viscosity, the uncertainty in kinematic viscosity can be neglected.

#### Confidence interval of calculated aircore depth

Applying the theory of error propagation to Eq. (11), the confidence interval  $\delta H_D$  is calculated by:

$$\delta H_D = \pm \sqrt{\left(\left|\frac{\partial H_D}{\partial \Gamma}\right| \delta \Gamma\right)^2 + \left(\left|\frac{\partial H_D}{\partial Q}\right| \delta Q\right)^2 + \left(\left|\frac{\partial H_D}{\partial H}\right| \delta H\right)^2 + \left(\left|\frac{\partial H_D}{\partial D}\right| \delta D\right)^2}$$

and by taking the derivatives:

$$\delta H_D = \pm \sqrt{\left(\left|\frac{\partial H_D}{\partial \Gamma}\right| \delta \Gamma\right)^2 + \left(\frac{0.0625\Gamma^2}{\pi^3 D^2 H g (v + k\Gamma)}\right)^2 \left(\delta Q^2 + \left(\frac{Q\delta H}{H}\right)^2 + \left(\frac{2Q\delta D}{D}\right)^2\right)}$$

By evaluating the contributions of the different uncertainties the equation is reduced to:

$$\delta H_D = \pm \sqrt{\left(\frac{H_D(\Gamma + d\Gamma) - H_D(\Gamma)}{d\Gamma}\right)^2 \delta \Gamma^2 + H_D^2 \left(\frac{0.002Q}{D}\right)^2} \quad (13)$$

Inhere, the term  $\partial H_D/\partial \Gamma$  is calculated numerically because of its complex differential form. Using Eq. (13), the confidence interval of the calculated aircore depth is about 10%.

## EXPERIMENTAL RESULTS AND DISCUSSION

Experiments are conducted at different flow rates and circulation values and with a constant undisturbed water depth of 0.90 m and outlet diameter 0.044 m. Figure 6 shows photos of the vortex at flowrates 2.5, 3.15 and 4.3 m<sup>3</sup>/h. The figures shows clearly the wider shape of the aircore at higher circulation but equal flow rate which is due to the higher bulk tangential velocity. The photos also show some gravity waves on the aircore giving the aircore a corkscrew shape. These waves can play a major role in the research to the ability of transporting floating material as discussed later.

When pouring dye in the aircore a hollow cylinder was formed around the vortex core (Figure 7) which was also observed by Echávez (2002). The presence of this relatively stable hollow dye core indicates that there is no or very small radial inflow into the core and that there is less turbulent dissipation in radial direction. It was also observed that when pouring dye close to the bottom outlet a dye cylinder was formed around the vortex core indicating the presence of an upward flow. Both observations need special attention as it can play a major role in analysing the axial and radial velocity profiles around the vortex core.

### Experimental aircore depth

Figure 8 shows the experimental aircore depths at different flowrates and circulation values. These experimental results are important for verification of the theoretical vortex models as their formulas of the axial and radial velocity profiles forms the base of the vortex transport model. According to this experimental set-up it's clearly visible that the aircore depth is much more sensitive to the flow rate as to the circulation. It was also experimentally observed that a sudden increase (within a few seconds) of the flow rate leads to a very rapid growth of the aircore depth. As the circulation in the tank is considered as constant during this observation due to the inertia of the water mass in the tank, this phenomenon must be related to the increase of velocity in the outlet i.e. higher flowrate.

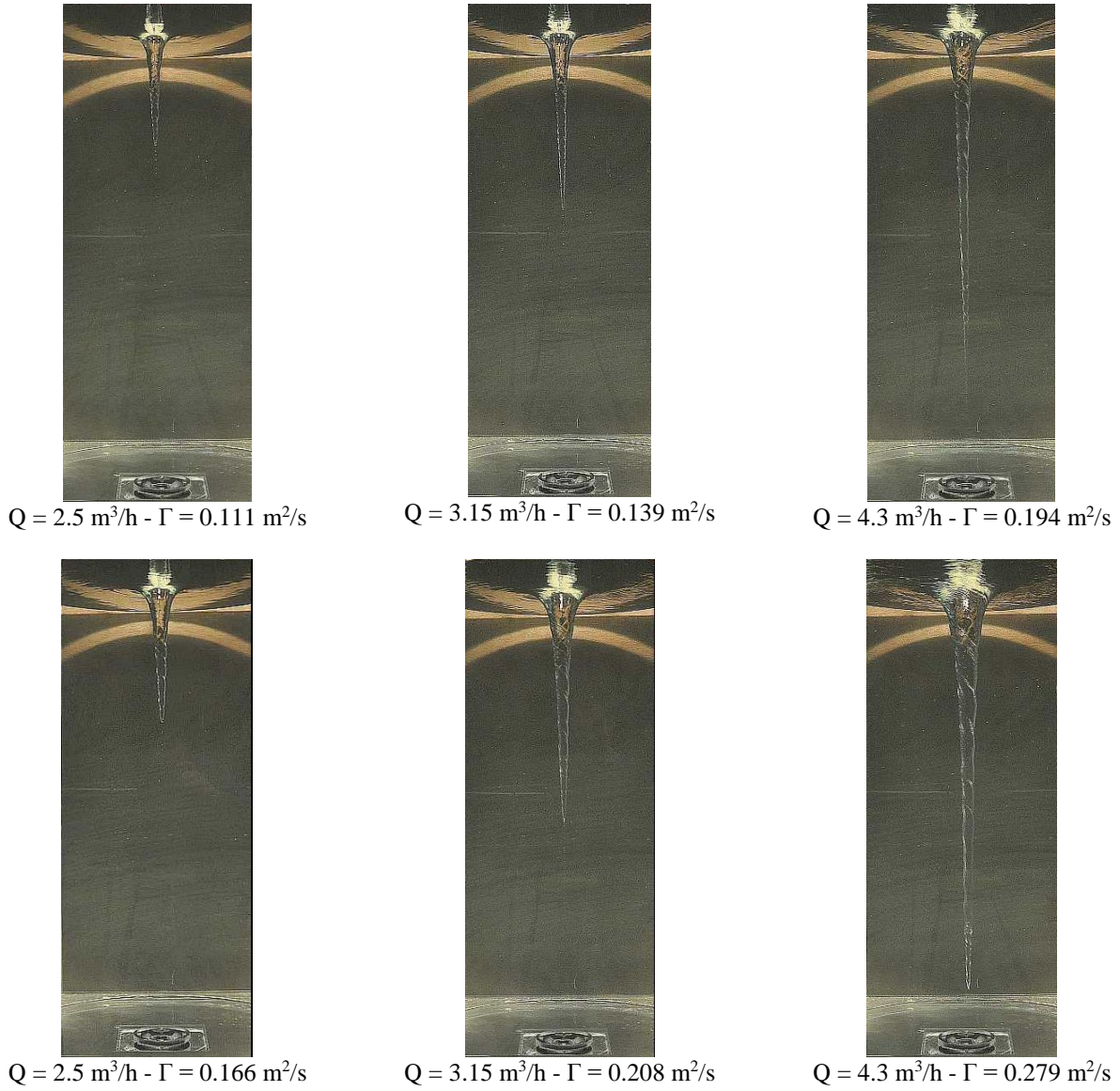


**Figure 6** Vortex aircore shape as function of flowrate and (bulk)circulation with outlet diameter  $D = 0.044 \text{ mm}$ . Due to gravity waves, some aircore shows a corkscrew shape

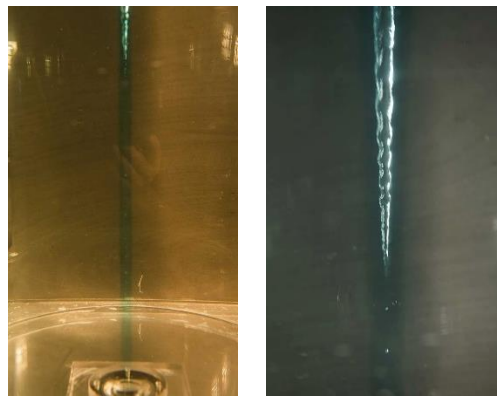


**Figure 7** Presence of hollow dye cylinder around aircore and vortex core

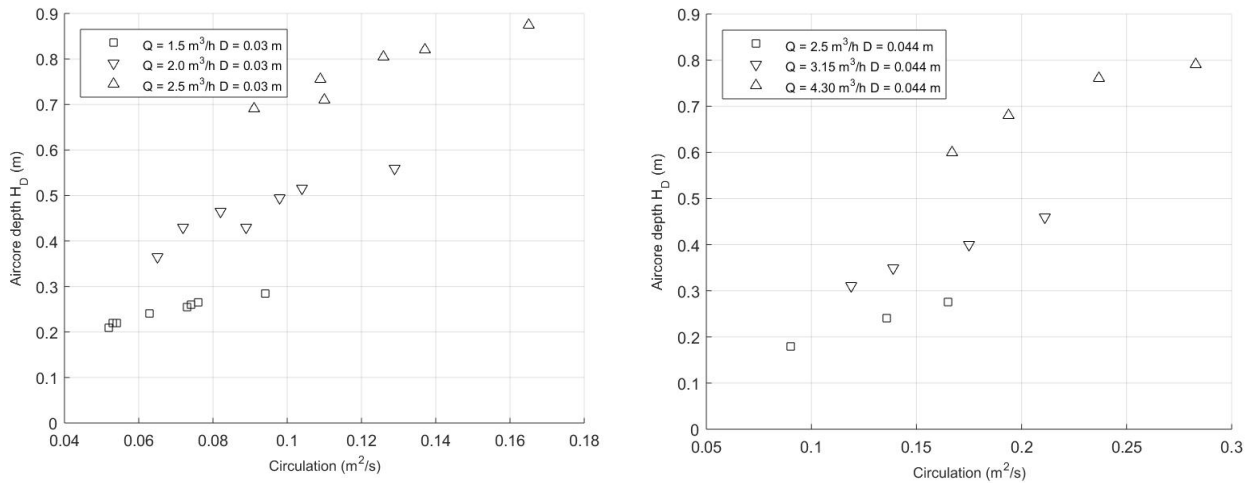


**Figure 8** Experimental vortex aircore depths at different outlet diameters and flow rates with outlet diameter  $D = 0.03$  m in left graph and  $D = 0.044$  m in right graph.

### Vortex models aircore depth

In Figure 9 the experimental aircore depths are compared with the calculated aircore depths with the Burgers/Odgaard and the Hite & Mih vortex model. The calculated aircore depth is limited to the undisturbed water depth. It's clearly visible that both models doesn't match the experimental results: the Burgers/Odgaard model highly overestimates the aircore depth (at  $Q = 4.3$  m<sup>3</sup>/h all aircore depths were much larger than 0.90 m) where the Hite & Mih model shows an underestimation. However, the Hite & Mih model shows a much better agreement than the Burgers/Odgaard model.

As both models uses the same eddy viscosity model  $\nu_t = \nu + k\Gamma$ , it's reasonable to exclude this modelling approach as the main cause of the models imprecision. The main difference between both models is the width of the core radius  $r_c$  witch is smaller in the Burgers/Odgaard model resulting in higher concentrated vorticity and thus larger aircore depth as shown. The core radius is determined from the axial velocity expression were this expression is derived by substituting the expression of the radial velocity in the continuity equation. The Burgers/Odgaard model calculates the radius assuming a radial velocity of  $V_r = -ar$  at  $r < r_c$  and thus  $V_z = 2az$  to satisfy continuity. This means that in the core  $\partial V_z / \partial r = 0$ . However, Echávez (2002) showed that the maximum axial velocity occurs at the vortex centre and decreases with increasing radius fortifying that  $\partial V_z / \partial r \neq 0$ . Indeed, a radial distribution of the axial velocity is present in the Hite & Mih model and therefore providing a better match. On the other hand the dye showed the presence of a stationary hollow cylinder around the vortex core (Figure 7) assuming no or very less radial inflow into the vortex core which was also stated by Echávez (2002). Based on continuity this means that the  $\partial V_z / \partial z = 0$  which is a contradiction with most general vortex models.

Knowledge of the radial and axial velocity distribution is essential to determine the transport ability and capacity of the free surface vortex. Therefore, the vortex velocity field will be measured with laser particle image velocimetry (PIV) providing experimental data giving highly valuable insight in the vortex flow around the core.

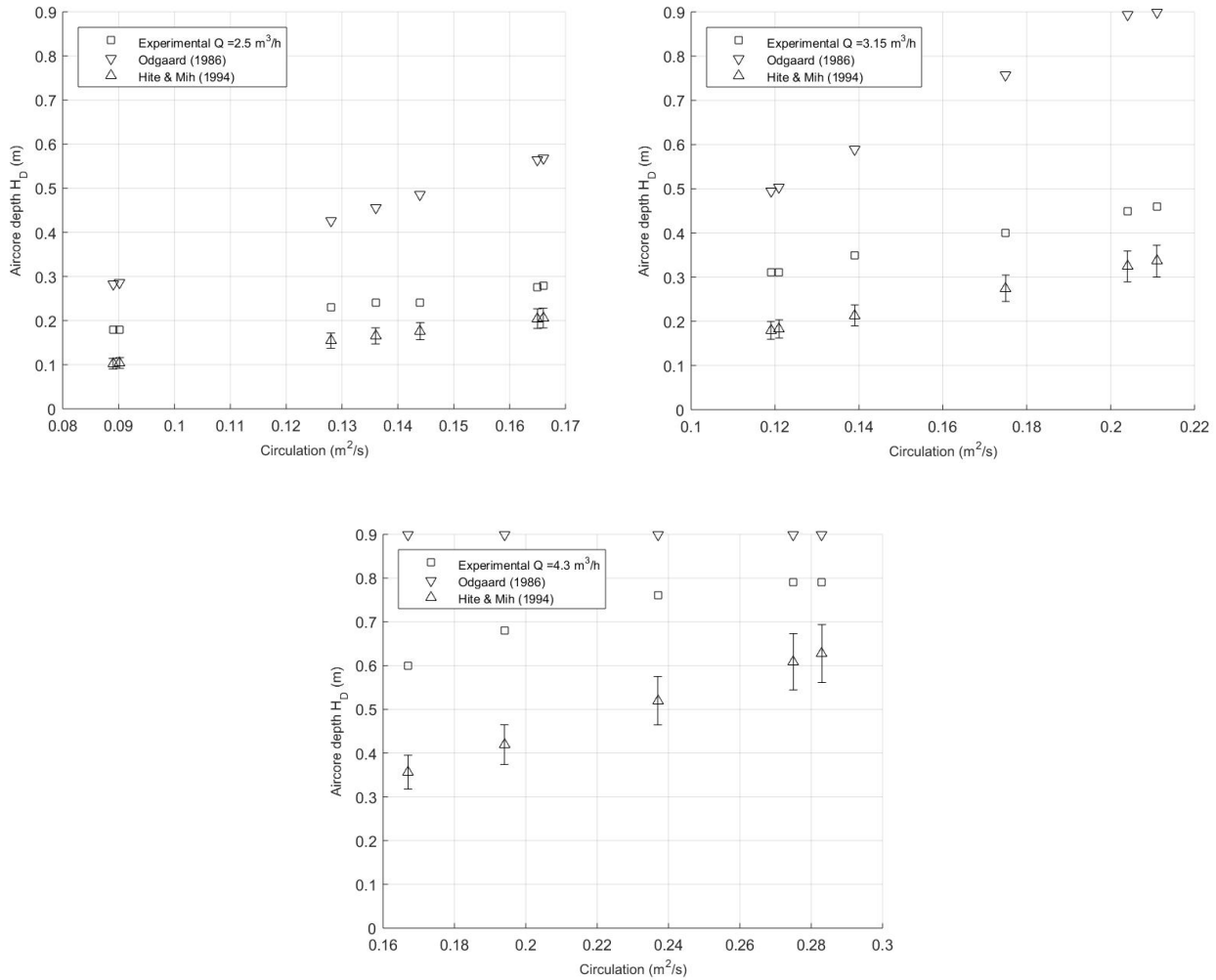


**Figure 9** Calculated aircore depth with the Burgers/Odgaard model and the Hite & Mih model versus experimental aircore depth at flow rates 2.5, 3.15 and 4.3  $m^3/h$ . Calculated values are limited to the undisturbed water depth  $H=0.90$  m.

**Vortex transport experiments**

Experiments are conducted with different floating particles for a qualitative investigation of the free-surface vortex transport ability. The used particles are  $\text{\O}4$  mm PE pearls,  $\text{\O}20$  mm hollow plastic balls and  $20 \times 20 \times 20$  mm wooden cubes with densities of respectively  $\pm 20$ ,  $\pm 700$  and  $\pm 600 \text{ kg/m}^3$ . Holes are drilled in a few  $\text{\O}20$  mm balls to fill the balls with water increasing the density nearly equal to water.

First, the total water surface was covered with a layer of PE pearls. The combination of cohesive forces and surface tension sticks the pearls together and forming a coalesced floating layer forming a severe condition for transport. Indeed, the layer first rotates slowly as a solid body but after a while the pearls starts rotating as irrotational flow and a free-surface vortex is formed. The vortex starts transporting the pearls as shown in Figure 10 A. As the vortex aircore depth grows due to increasing circulation, the transport rate of the pearls decreases (Figure 10 B). When the vortex is stable i.e. constant aircore depth, transport of pearls has stopped (Figure 10 C). The axial velocity introduces not sufficient drag force to overcome the buoyancy force of the pearls.

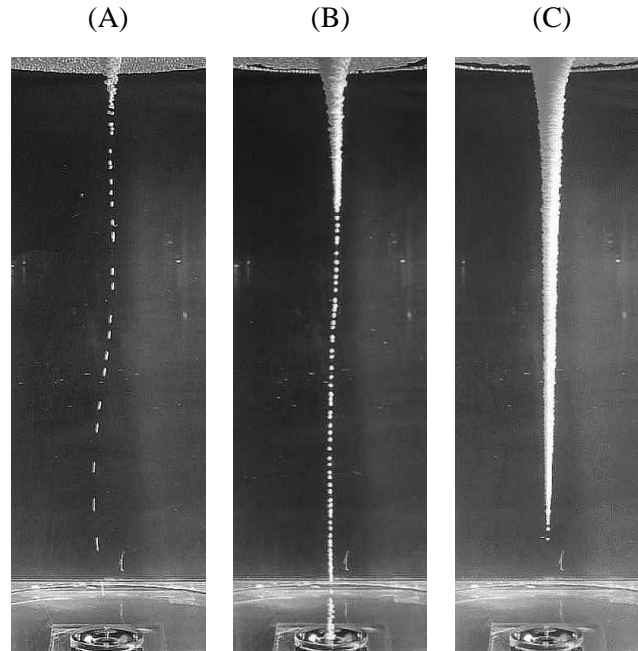


**Figure 10** Transport stages of  $\text{\O}4$  mm PE pearls starting with a coalesced floating layer of the pearls.

Experiments with individual particles shows some interesting phenomena's. At different vortex strength i.e. aircore depths, individual 20 mm balls were placed on the water surface next to the vortex. The high radial inflow at the surface pushes the ball into the vortex. After following the aircore in downward direction by a spirally movement some strange phenomena was observed. When approaching the end of the aircore, and what was observed as a random process, the ball would either (1) stick in the aircore centre (Figure 11, B) or in the solid core (Figure 11, C) rotating on its own centre of mass, or (2) the ball showed a translating movement around the vortex core and a downward movement to the outlet so transport is present (see Figure 11, A and B). Both phenomena's were observed at a substantial number of different combinations of flow rate and circulation and no distinct combination was determined where only one of the phenomena's was present. However, a small disturbance (or source of the waves) in the gravity waves on the aircore surface (see Figure 6) seems to affect the movement of the ball whether to be captured in the aircore or vortex core or starts translating around the vortex core. This preliminary observation will be further investigated with use of the PIV measurements.

The same experiments as with the  $\text{\O}20$  mm ball were conducted with the 20 mm wooden cube to investigate the effect of the particle shape. The experiments never showed a translating transport and the cube was always captured in the aircore of solid core.

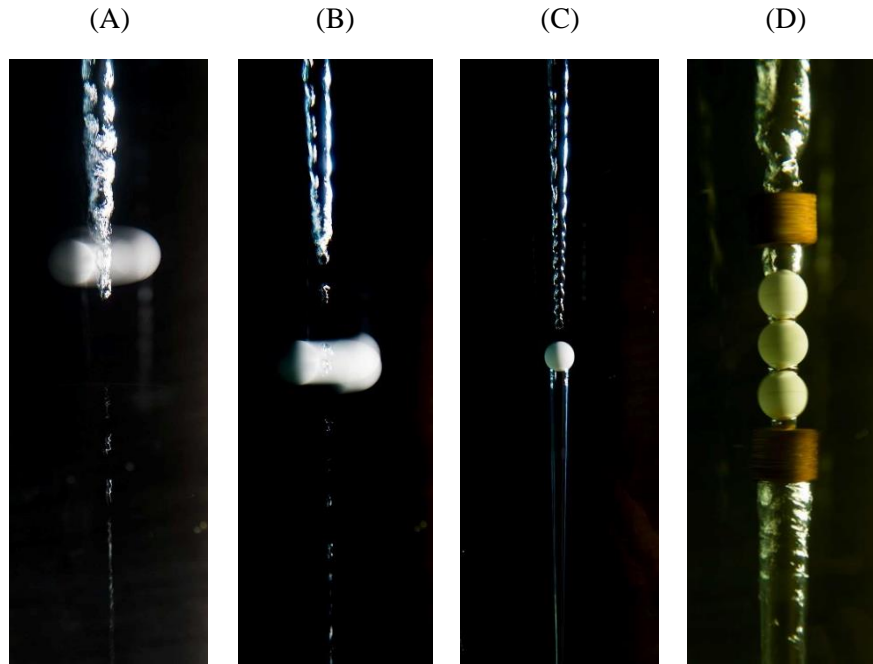


**Figure 11** Observed transport phenomena Photo A: translating and transporting particle around aircore, photo B: translating and transporting particle around solid core subsequent to first photo, photo C: rotating particle in vortex core pushing air downwards and photo D: rotating particles in aircore

Experiments with the Ø20 mm balls filled with water revealed that as the particle density approaches the density of water, particles will be ejected from the vortex aircore area due to unbalance between radial drag force and centrifugal force and seems independent of the vortex characteristics. Furthermore, some experiments showed that the ejected ball starts rotating at large distance around the vortex. As the ball approximately stays on the same radial distance, there is a balance between centrifugal force and radial drag force. Hence, we may assume that there is some (small) radial flow throughout the horizontal plan at large distance from the aircore.

## CONCLUSIONS

Experiments are conducted to investigate the transport ability of free-surface vortices. Experimental results i.e. the aircore depth are compared with two theoretical vortex models: the Burgers (1948)/Odgaard (1986) model and the Hite & Mih (1994) model. Where the Burgers/Odgaard model overestimates the aircore depth, the Hite & Mih model underestimates the aircore depth but shows a better agreement. The aircore depth has shown to be very sensitive to a sudden decrease in flowrate at stationary (bulk) circulation and therefore it seems reasonable to conclude that the accuracy of models strongly depends on the correct modelling of the axial and radial velocity profiles and needs more (experimental) research.

Besides the correct calculation of the aircore depth, enhanced knowledge of the axial and radial velocity profiles around the vortex is essential to determine the vortex transport capacity: whereas a free-surface vortex is able to transport buoyant material without the entrainment of air, the transport efficiency is shown to be highly sensitive to the flow field around the vortex aircore i.e. the radial and axial drag forces acting on the particle as function of the shape and density of the particle. Based on this the vortex transport capacity  $VT$  can be written as  $VT = f(V_z(r,z), V_r(r,z), \beta, C_D(r,z), \rho_m, v_t)$  with

$\beta$  a particle shape parameter describing the surface in radial and axial direction where drag occurs,  $C_D(r,z)$  the drag coefficient in radial and axial direction and  $\rho_m$  the particle density.

Extensive future research will be conducted by the author on the observed phenomena's as they are essential in determine the ability and capacity of free-surface vortices as mechanism for transport of floating debris in wastewater pump sumps. For instance, with use of PTV and laser PIV the velocity profiles will be determined in detail to obtain better data of the flow pattern in the vortex (core) for analysing the phenomena of the transported particle to be captured in the core or being transported to the outlet.

### ACKNOWLEDGEMENT

This experimental research work is financed by the Municipality of Rotterdam, departments Engineering Consultancy and Water, the Netherlands.

### REFERENCES

- Anwar, H.O. 1966. Formation of a Weak Vortex, *Journal of Hydraulic Research*, 4:1, 1-16.
- American National Hydraulic Standards Institute (2012). American National Standard for rotodynamic pumps for pump intake design. ANSI 9.8-2012. ISBN 978-880952-70-2.
- Brocard, D.N., Beauchamp, C.H., Hecker, G.E. (1983). Analytic Predictions of Circulation and Vortices at Intakes. Alden Research Laboratory, Research Project 1199-8.
- Burgers J.M. (1984). A Mathematical Model Illustrating the Theory of Turbulence, *Advances in Applied Mechanics*, 1, 171–199.
- Dagget, L.L. and Keulegan, G.H. 1974. Similitude in Free Surface Vortex Formations, *Journal of Hydraulics Division, Proc. A.S.C.E.*, Vol. 100, No. HY 11, 1565-1581.
- Echávez, G. and McCann, E. 2002. An experimental study on the free surface vertical vortex, *Experiments in Fluids* 33, 414-421.
- Gulliver, S., Rindels, A.J. (1987). Weak Vortices at Vertical Intakes. *J. Hydraul. Eng.*, 1987.113, 1101-1116
- Hite, E.J., Mih, W.C. (1994). Velocity of Air-Core Vortices at Hydraulic Intakes. *J. Hydraul. Eng.*, 120(3), 284-297.
- Korving J.L., Clemens F.H.L.R., and van Noortwijk J.M. (2006b). Statistical Modelling of the Serviceability of Sewage Pumps. *Journal of Hydraulic Engineering*, 2006.132, 1076-1085.
- Mih, W.C. (1990). Discussion of Analysis of fine particle concentrations in a combined vortex. *J. Hydraul. Res.*, 28(3), 392-395.
- Odgaard, A. J. (1986). Free-surface air core vortex. *J. Hydraul. Eng.*, 10.1061, 610–620.
- Rankine, W.J.M. (1858). *Manual of Applied Mechanics*. C. Griffen Co., London.
- Rosenhead, L. (1930). The spread of vorticity in a wake behind a cylinder. *Proc., Royal Society of London, England, Series A*, 127, 590-612.
- Suerich-Gulick, F., Gaskin, S.J., Villeneuve, M. Parkinson, E. (2014a). Characteristics of Free Surface Vortices at Low-Head Hydropower Intakes. *Journal of Hydraulic Engineering*, 2014.140, 291-299.